Pearling instability of a cylindrical vesicle

Gwenn Boedec, Marc Jaeger, Marc Leonetti

Pearling instability of a cylindrical vesicle

G. Boedec[1,†], M. Jaeger[2] and M. Leonetti[1]

[1]Aix-Marseille Université, CNRS, IRPHE UMR 7342, Centrale Marseille, Technopôle de Château-Gombert, 49, Rue Frédéric Joliot-Curie, 13384 Marseille, France

[2]Aix-Marseille Université, CNRS, M2P2 UMR 7340, Centrale Marseille, Technopôle de Château-Gombert, 38, Rue Frédéric Joliot-Curie, 13451 Marseille, France

A cylindrical vesicle under tension can undergo a pearling instability, characterized by the growth of a sinusoidal perturbation which evolves towards a collection of quasi-spherical bulbs connected by thin tethers, like pearls on a necklace. This is reminiscent of the well-known Rayleigh–Plateau instability, where surface tension drives the amplification of sinusoidal perturbations of a cylinder of fluid. We calculate the growth rate of perturbations for a cylindrical vesicle under tension, considering the effect of both inner and outer fluids, with different viscosities. We show that this situation differs strongly from the classical Rayleigh–Plateau case in the sense that, first, the tension must be above a critical value for the instability to develop and, second, even in the strong tension limit, the surface preservation constraint imposed by the presence of the membrane leads to a different asymptotic behaviour. The results differ from previous studies on pearling due to the consideration of variations of tension, which are shown to enhance the pearling instability growth rate, and lower the wavenumber of the fastest growing mode.

Key words: interfacial flows (free surface), low-Reynolds-number flows, membranes

1. Introduction

Thin liquid threads are ubiquitous: from engineering processes such as electrospinning, ink-jet printers, fibre coating, to everyday phenomena such as the jet formed by impact on a liquid sheet or water dripping from a faucet. They are observed in a large range of scales: from micrometric jets in microfluidic chips to large-scale jets in astrophysics (for a recent review on physics of liquid jets, see e.g. Eggers & Villermaux 2008). Despite the wide range of Reynolds number covered by these examples, all jets show striking similarities in the sense that the straight cylindrical shape is unstable and leads ultimately to drop formation and fragmentation of the jet. The driving mechanism of this instability is the surface tension: perturbations of the jet radius decreasing its area will grow. Any perturbation whose wavelength is larger than the perimeter of the jet decreases its surface energy (Plateau 1873), and is thus unstable. This energetic argument does not give any information about the growth rate of the perturbations. However, dynamics and stability of liquid threads are of primary

† Email address for correspondence: boedec@irphe.univ-mrs.fr

importance since some applications require a stable (or long-lived) jet (e.g. fibre formation by electrospinning), while others aim towards the rapid fragmentation of the jet in drops (e.g. atomization of a spray). Numerous studies have thus been devoted to the understanding of the dynamics of liquid columns, considering various properties of the liquid and of its surrounding environment.

The first case studied was that of a column of Newtonian fluid with constant surface tension: the pioneering work of Rayleigh tackles both the inertia dominated jet (Rayleigh 1878) and the viscosity dominated jet (Rayleigh 1892*b*). The effect of the external media was only considered for inviscid fluids in the limit case where inertia of surrounding fluid is greater than that of the jet Rayleigh (1892*a*). This analysis was later refined by Tomotika (1935), in the viscosity-dominated regime, by taking into account an external fluid of arbitrary viscosity. While the Rayleigh analysis for the viscous case (Rayleigh 1892*b*) predicts that the fastest growing wavenumber k_{max} is equal to zero (homogeneous perturbation), Tomotika (1935) showed that taking into account the external media leads to a finite value for the most unstable wavelength ($k_{max} \neq 0$), since the external viscosity damps large-scale flow associated with infinite wavelength perturbations.

Even slight deviations from this Newtonian case with constant surface tension can change radically the picture: taking into account the influence of surfactants at the interface leads to strong modification of the dispersion relation, in particular in the viscosity-dominated regime (Palierne & Lequeux 1991; Hansen, Peters & Meijer 1999; Timmermans & Lister 2002). For example, Timmermans & Lister (2002) showed that strong surfactant effects can suppress capillary instability in the long-wavelength limit even without surrounding fluid, thus leading to a $k_{max} \neq 0$. The effect of surfactant was found to be less important as the importance of inertia grows, with negligible effect for $Re \to \infty$ as already noted by Whitaker (1976).

Considering the possible viscoelastic effects in the bulk of the fluid leads to complex effects. First, the breakup of the liquid thread can be significantly delayed (Amarouchene *et al.* 2001) by the addition of polymers in the liquid. Moreover, columns of viscoelastic liquids display a characteristic pattern of 'beads on a string' (e.g. Oliveira & McKinley 2005; Clasen *et al.* 2006; Ardekani, Sharma & McKinley 2010; Bhat *et al.* 2010).

Finally, another situation of interest is the case where the interface between the two liquids is covered by a material different from the surrounding fluids, such as a phospholipidic bilayer. This situation is typical of biologically inspired systems such as vesicles, which are essentially drops enclosed by a membrane. This closed membrane is formed by self-assembly of phospholipids into a bilayer structure, which is the main component of cell membranes, and gives them resistance to bending as well as surface incompressibility. As such, a vesicle is a model system which is widely studied to gain insight into cell behaviour under stress, in particular to understand red blood cells dynamics in blood flow. However, even if vesicles membrane and red blood cells membrane are very similar (both are surface incompressible and resist bending), red blood cells are more complex objects (Vlahovska, Podgorski & Misbah 2009) since their inner fluid is non-Newtonian and the membrane also resist shearing due to the spectrin network. Vesicles are also an interesting system from the fluid mechanics point of view, since the presence of the membrane leads to very different dynamics when compared with surface-tension-driven dynamics, highlighting the crucial role of the interface. In particular, the formation of a pattern very similar to the 'beads on string' has been observed on cylindrical vesicles enclosing Newtonian fluids. This pearling instability can be triggered either by application of a laser tweezer

(Bar-Ziv & Moses 1994; Bar-Ziv *et al.* 1997, 1998, 1999), by application of an extensional flow (Kantsler *et al.* 2008), by modification of the spontaneous curvature (Chaïeb & Rica 1998; Tsafrir *et al.* 2001; Campelo & Hernández-Machado 2007), by application of a magnetic field on ferromagnetic vesicles (Ménager *et al.* 2002) or by osmotic pressure (Yanagisawa *et al.* 2008; Sanborn *et al.* 2013). Theoretical analysis of the laser-induced instability has been done assuming that the laser induced a constant tension (Nelson *et al.* 1995; Goldstein *et al.* 1996; Gurin, Lebedev & Muratov 1996; Powers 2010), or either a time-dependent tension (Granek & Olami 1995) or tension gradients (Olmsted & MacIntosh 1997). The details of the analysis published in Nelson *et al.* (1995) were reported in Goldstein *et al.* (1996), and corrected later in Powers (2010). Note that the result reported in Powers (2010) (neglecting the membrane viscosity contribution) is the same as the result reported in Gurin *et al.* (1996) (for fluids of equal viscosities). The constant tension analysis of Nelson *et al.* (1995) and Goldstein *et al.* (1996) was then used to predict the front velocity of the pearling instability (Bar-Ziv *et al.* 1997; Powers & Goldstein 1997). On the other hand, Goveas, Milner & Russel (1997) considered the evolution of the system when pearls are formed and drift towards the laser trap.

Despite the difference between surfactant-covered threads and cylindrical vesicles, their behaviour should share a common limit: surfactant-covered threads with strong surfactant effects, leading to an effective surface incompressibility constraint should behave as cylindrical vesicles without bending resistance, corresponding to the strong tension limit. However, none of the previous work on vesicles (Nelson *et al.* 1995; Goldstein *et al.* 1996; Gurin *et al.* 1996; Powers 2010) recovers the incompressible interface limit of surfactant covered threads analysis (Palierne & Lequeux 1991; Timmermans & Lister 2002). Driven by this discrepancy, we calculate in this paper the growth rate of the pearling instability assuming a constant tension of the membrane in the base state. This leads to a different expression for the growth rate compared with Nelson *et al.* (1995), Goldstein *et al.* (1996), Gurin *et al.* (1996) and Powers (2010), but as we discuss in § 4, our analysis recovers the aforementioned results if tangential equilibrium is neglected. Furthermore, the complete result presented here matches the incompressible interface limit of surfactant-covered threads analysis (Palierne & Lequeux 1991; Timmermans & Lister 2002).

The paper is organized as follows. In § 2, we introduce the system considered, and write the equations describing the problem. The linear stability analysis is then detailed in § 3. Finally, results obtained are discussed in § 4, with particular attention paid to the limit case of an incompressible interface.

2. System

2.1. *Vesicle under flow*

We consider a cylindrical column of fluid immersed in another fluid (see figure 1), with a phospholipidic membrane located at the interface between the two fluids. This is a model for situations commonly encountered for vesicles: cylindrical vesicles can be formed with a proper experimental protocol (Bar-Ziv *et al.* 1998; Kantsler *et al.* 2008), and cylindrical tethers on quasi-spherical vesicles can be easily formed by the application of a point-like force (Evans *et al.* 1996; Fygenson, Marko & Libchaber 1997) or by the application of hydrodynamic stresses (Boedec *et al.* 2013; Zhao & Shaqfeh 2013).

The hydrodynamical description of the complete system requires us to describe both the hydrodynamical fields in the inner and outer fluid, as well as the coupling

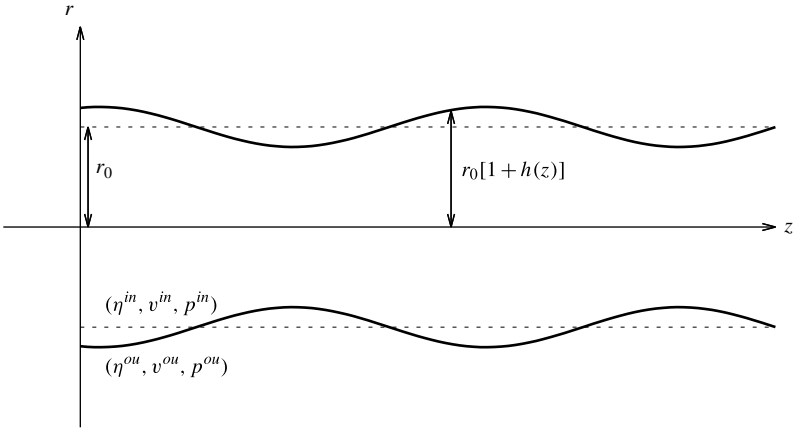

FIGURE 1. Scheme of the system considered here: the evolution of the perturbations on a cylindrical interface separating two fluids is investigated taking into account the presence of a phospholipidic membrane at the interface.

conditions between these fields at the interface, which are related to the membrane properties. Due to the typical length scale $R_0 \sim 10\ \mu$m, the evolution of a vesicle into an otherwise quiescent fluid is correctly described within the Stokes approximation for the inner and the outer fluid:

$$\left.\begin{aligned} \eta \Delta \boldsymbol{v} - \nabla p = \boldsymbol{0} \\ \nabla \cdot \boldsymbol{v} = 0 \end{aligned}\right\} \tag{2.1}$$

where $(\boldsymbol{v}, p)$ are the velocity and pressure fields, and η is the dynamic viscosity.

At the interface, the velocities are continuous:

$$\boldsymbol{v}^{in}(\boldsymbol{x}) = \boldsymbol{v}^{out}(\boldsymbol{x}) \tag{2.2}$$

where the superscripts *in* and *out* denote the inner and outer fields, and $\boldsymbol{x}$ is the position of the interface. Since the membrane is impermeable, there is no flow through it, and the position of the interface evolves as

$$\frac{\partial \boldsymbol{x}}{\partial t} = \boldsymbol{v}^{in}(\boldsymbol{x}) = \boldsymbol{v}^{out}(\boldsymbol{x}). \tag{2.3}$$

Finally, the hydrodynamical description is closed by writing the mechanical equilibrium of the membrane:

$$[\![\sigma]\!] \cdot \boldsymbol{n} + \boldsymbol{f^m} = 0, \tag{2.4}$$

where $\boldsymbol{n}$ is the outward normal to the interface, $[\![\sigma]\!] = [\sigma^{out} - \sigma^{in}]$ is the jump in the Newtonian stress tensor $\sigma = -p\boldsymbol{I} + 2\eta \boldsymbol{D}$, with $\boldsymbol{D} = 1/2\left(\nabla \boldsymbol{v} + \nabla^{\mathrm{T}} \boldsymbol{v}\right)$ the strain rate tensor. In the above equation, $\boldsymbol{f^m}$ stands for the surface density of force related to the membrane mechanics.

For a vesicle, two membrane properties are crucial when considering the interface response to deformation by hydrodynamical stresses. First, the interface is composed of a different material from the bulk fluids (namely, phospholipids). Since there is no exchange of phospholipids between the interface and the fluids, and since

the coefficient of compressibility of the phospholipid bilayer is very high, a usual assumption in vesicle dynamics studies is that the surface density of phospholipids is conserved. The direct consequence is that the velocity field must be surface divergence free:

$$\boldsymbol{\nabla}_s \cdot \boldsymbol{v}^{in} = \boldsymbol{\nabla}_s \cdot \boldsymbol{v}^{out} = 0, \tag{2.5}$$

where $\boldsymbol{\nabla}_s$ is the surface gradient.

Second, there is a cost to deform the membrane, which is usually modelled with the Helfrich free energy:

$$F = \int_S \left[\frac{\kappa}{2}(2h)^2 + \gamma \right] \mathrm{d}S, \tag{2.6}$$

where $\kappa \sim 20\ k_B T$ (Dimova *et al.* 2006) is the bending modulus of the interface, h is the mean curvature and γ is a surface Lagrange multiplier which enforces the constraint of surface incompressibility (2.5). Here γ has the dimension of a surface tension, but is not a material parameter: it is a supplementary unknown of the problem which must be determined. Physically, γ is the equivalent of the pressure in the bulk for incompressible fluids: it represents the non-deviatoric part of the membrane stress tensor Σ, namely $\gamma = (\Sigma_{\theta\theta} + \Sigma_{zz})/2$.

Surface density of force $\boldsymbol{f^m}$ is thus given by the first variation of Helfrich energy:

$$\boldsymbol{f^m} = -\frac{\delta F}{\delta \boldsymbol{x}} = \boldsymbol{\nabla}_s \gamma + \{2\gamma h - \kappa[2\Delta_s h + 4h(h^2 - k_G)]\}\boldsymbol{n}, \tag{2.7}$$

where Δ_s is the Laplace–Beltrami operator, k_G is the Gaussian curvature and we use the convention such that $h = -1/r < 0$ for a straight cylinder.

2.2. *Base state and physical mechanism of the pearling instability*

Assume a cylindrical vesicle of radius r_0 and infinite length, under tension γ. Thus, the mechanical equilibrium of the membrane can be written

$$p^{in} - p^{out} = \frac{\gamma}{r_0} - \frac{\kappa}{2r_0^3}. \tag{2.8}$$

Thus, a solution satisfying the set of (2.1)–(2.5) is

$$\left.\begin{aligned} \boldsymbol{v}^{in} = \boldsymbol{v}^{out} &= \boldsymbol{0} \\ p^{out} &= 0 \\ p^{in} &= \frac{\kappa}{r_0^2}\frac{1}{r_0}\left[\frac{r_0^2}{\kappa}\gamma - \frac{1}{2}\right] \end{aligned}\right\}. \tag{2.9}$$

In (2.9), it is clear that for $\gamma = \kappa/2r_0^2$, the inner pressure is zero as well. This is the classical relationship between tension and radius of the cylinder for equilibrium tethers pulled out of vesicles by point-like forces (Evans *et al.* 1996; Fygenson *et al.* 1997) or hydrodynamical stresses (Boedec *et al.* 2013; Zhao & Shaqfeh 2013).

We consider here the stability of this configuration when the radius is perturbed. The exact linear stability analysis of the full system described in § 2.1 is postponed to § 3, while here and in the following § 2.3 we will make some strong simplifications to highlight the driving mechanism of the instability. We thus neglect the effect of the

outer fluid, and focus on the evolution of p^{in} as written in (2.9). Inserting the ansatz $r = r_0(1 + \tilde{\delta r})$ in (2.9), one finds

$$\delta p^{in} \approx \tilde{\delta r} \left(\frac{3\kappa}{2r_0^3} - \frac{\gamma}{r_0} \right). \tag{2.10}$$

There is thus a pressure gradient between the 'necks' ($\tilde{\delta r} < 0$) and the 'pearls' ($\tilde{\delta r} > 0$), whose sign depends on the value of the tension: if $\gamma < 3\kappa/2r_0^2$, the pressure gradient will lead to a flow from the pearls to the necks, and perturbations will be damped. If $\gamma > 3\kappa/2r_0^2$, perturbations will be amplified by the flow. This prompts us to choose as a control parameter of the instability the value of the tension in the base state, which we will denote hereafter as γ^0. In this simple analysis, we have neglected variations of tension, which we will discuss in the following section.

2.3. *Effect of gradients of tension*

To discuss the effect of the variation of the tension in the case of a vesicle, one needs to first estimate this variation. In contrast to a surfactant-covered thread, the tension is not given by an equation of state, but is the Lagrange multiplier associated with the constraint of incompressibility. Thus, if there is no flow, the tension is constant. The previous 'static' analysis is then not applicable directly. However, it is possible to discuss whether the tension gradients enhance or dampen the instability by considering the dominant terms of the flow. Assuming a thin cylinder slightly deformed, and neglecting the outer fluid, one can write the inner flow in the lubrication approximation:

$$\left.\begin{aligned} u(r,z) &= -\frac{r}{2}\frac{\partial v_0(z)}{\partial z} - \frac{r^3}{16\eta}\frac{\partial^2 p}{\partial z^2} + \cdots \\ v(r,z) &= v_0(z) + \frac{r^2}{4\eta}\frac{\partial p}{\partial z} + \cdots \end{aligned}\right\} \tag{2.11}$$

where u, v are the radial and axial component of the velocity, and v_0 is the axial component of the velocity at the centre of the cylinder ($r = 0$). The surface incompressibility constraint imposes $\partial u/\partial r = 0$, which gives

$$v_0 = -\frac{3r_0^2}{8\eta}\frac{\partial p}{\partial z} \Rightarrow v(r,z) = \frac{1}{4\eta}\frac{\partial p}{\partial z}\left(r^2 - \tfrac{3}{2}r_0^2\right). \tag{2.12}$$

As stated previously, the tension of a vesicle membrane acts exactly as the pressure in the bulk. To determine its variation, one can use the mechanical equilibrium in the tangent direction, which gives

$$\nabla_s \gamma = -(\boldsymbol{Id} - \boldsymbol{n} \otimes \boldsymbol{n}) \cdot [[\sigma]] \cdot \boldsymbol{n} \tag{2.13}$$

where $(\boldsymbol{Id} - \boldsymbol{n} \otimes \boldsymbol{n})$ is the projector onto the tangent plane. Using the flow field (2.11) with (2.12), this equation can be written as

$$\frac{\partial \gamma}{\partial z} = \frac{r}{2}\frac{\partial p}{\partial z}. \tag{2.14}$$

Using the previous analysis to determine the sign of the pressure gradient, it is clear that the tension is higher when the cylinder is pinched ('necks') and lower when the cylinder is expanded ('pearls'); see figure 2. As a result, the capillary pressure $\tilde{\delta r}(\gamma/r_0)$ is further increased in 'necks' and decreased in 'pearls', which strengthens the instability. Thus, the consideration of variations of tension leads to an enhancement of the instability. This counterintuitive result will be discussed further in § 4.

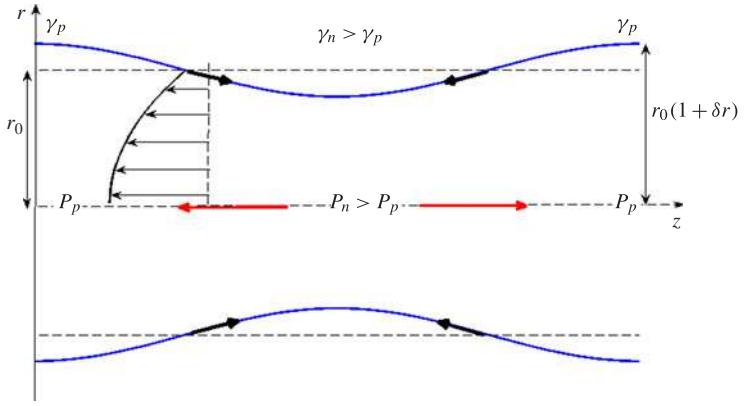

FIGURE 2. (Colour online) Effects of gradients of tension: the pressure gradient due to the capillary pressure leads to a Poiseuille flow, which generates viscous stresses on the interface. To ensure tangent mechanical equilibrium, gradients of tension develops, leading to a tension in the neck (γ_n) higher than in the pearls (γ_p). This increases the capillary pressure gradient, and thus increases the growth rate.

2.4. *Characteristic scales*

All dimensionless variables are designed with a capital letter. The radius of the cylindrical vesicle is chosen as the reference length scale $r = r_0 R$, $z = r_0 Z$. The tension is made dimensionless by the imposed tension γ^0, expressed in units of the equilibrium tension

$$\gamma = \gamma^0 \Gamma = \kappa/(r_0^2)\Gamma^0 \Gamma.$$

Velocities are made dimensionless by $V_0 = \gamma^0/\eta^{in} = \Gamma^0 \kappa/(\eta^{in} r_0^2)$, pressure is made dimensionless by $p_0 = \eta^{in} V_0/r_0$ and we choose as time scale $\tau = \eta^{in} r_0^3/(\kappa \Gamma^0)$. With these variables, the dimensionless system of equations to solve is

$$\left.\begin{array}{cc} \Delta \boldsymbol{V}^{in} - \boldsymbol{\nabla} P^{in} = \boldsymbol{0}, & \dfrac{1}{\lambda}\Delta \boldsymbol{V}^{out} - \boldsymbol{\nabla} P^{out} = \boldsymbol{0} \\ \boldsymbol{\nabla} \cdot \boldsymbol{V}^{in} = 0, & \boldsymbol{\nabla} \cdot \boldsymbol{V}^{out} = 0 \end{array}\right\} \tag{2.15}$$

where derivatives are taken with respect to dimensionless variables (R, Z) and where we have introduced the viscosity contrast $\lambda = \eta^{in}/\eta^{out}$. These equations are completed with the coupling conditions at the interface:

$$\left.\begin{array}{l} \left[-P^{out}\boldsymbol{I} + \dfrac{1}{\lambda}\left(\boldsymbol{\nabla}\boldsymbol{V}^{out} + \boldsymbol{\nabla}^{\boldsymbol{T}}\boldsymbol{V}^{out}\right) + P^{in}\boldsymbol{I} - \left(\boldsymbol{\nabla}\boldsymbol{V}^{in} + \boldsymbol{\nabla}^{\boldsymbol{T}}\boldsymbol{V}^{in}\right)\right] \cdot \boldsymbol{n} + \boldsymbol{F^m} = \boldsymbol{0} \\ \boldsymbol{\nabla}_s \cdot \boldsymbol{V}^{in} = 0, \quad \boldsymbol{\nabla}_s \cdot \boldsymbol{V}^{out} = 0 \\ \dfrac{\partial \boldsymbol{X}}{\partial T} = \boldsymbol{V}^{in} = \boldsymbol{V}^{out} \end{array}\right\} \tag{2.16}$$

where $\boldsymbol{F^m} = \boldsymbol{\nabla}_s \Gamma + \left\{2\Gamma H - 1/\Gamma^0\left[2\Delta_s H + 4H(H^2 - K)\right]\right\}\boldsymbol{n}$ is the dimensionless surface force density, $\boldsymbol{X} = \boldsymbol{x}/r_0$ is the dimensionless position of the interface and $T = t/\tau$ is the dimensionless time.

3. Linear stability analysis

In this section, we address the stability of the base state described in § 2.2: starting with a cylindrical vesicle of dimensionless radius 1 under tension Γ^0, we perturbate

the radius as

$$R(Z) = 1 + \delta R(Z) = 1 + \sum_k \delta R_k \mathrm{e}^{\mathrm{i}kZ} + \text{c.c.} \tag{3.1}$$

with $\|\delta R\| \ll 1$, and where c.c. is the complex conjugate of the sum. We then expand all quantities as follows:

$$\left.\begin{aligned} P &= P^0 + P^{\delta R} + O(\|\delta R\|^2) \\ V &= V^0 + V^{\delta R} + O(\|\delta R\|^2) \\ \Gamma &= \Gamma^0 + \Gamma^{\delta R} + O(\|\delta R\|^2) \end{aligned}\right\} \tag{3.2}$$

where f^0 denotes the variable f in the base state, and $f^{\delta R}$ is the variation at linear order of the variable f due to a change of radius δR. In the following, we compute the linear variation of all relevant quantities, and drop the superscript δR for clarity.

From a general point of view, the constraints of constant volume and constant membrane area are fulfilled as their variations are of the order of $O(\|\delta R\|^2)$.

3.1. *Hydrodynamics*

We begin the analysis with the computation of the velocity and pressure fields inside and outside a cylindrical tether. Taking the divergence of the Stokes equation, one finds that the pressure field is harmonic:

$$\frac{1}{R}\frac{\partial}{\partial R}\left(R\frac{\partial P}{\partial R}\right) + \frac{\partial^2 P}{\partial Z^2} = 0. \tag{3.3}$$

Looking for solution of the Laplace equation in cylindrical coordinates by the method of separation of variables, one finds

$$P(R, Z) = \sum_k [p_k I_0(kR) + p_k^* K_0(kR)]\mathrm{e}^{\mathrm{i}kZ} + \text{c.c.} \tag{3.4}$$

where c.c. stands for complex conjugate of the sum, p_k, p_k^* are the complex coefficients of the amplitudes of modes k and I_n, K_n are modified Bessel functions of the first and second kind of order n, which satisfy the modified Bessel differential equation

$$x^2\frac{\mathrm{d}^2 y}{\mathrm{d}x^2} + x\frac{\mathrm{d}y}{\mathrm{d}x} - (x^2 + n^2)y = 0. \tag{3.5}$$

Inserting the expression of the pressure field in the right-hand side of the Stokes equation with $\boldsymbol{V} = U\boldsymbol{e_r} + V\boldsymbol{e_z}$, one obtains

$$\left.\begin{aligned} &\frac{\partial}{\partial R}\left(\frac{1}{R}\frac{\partial (RU)}{\partial R}\right) + \frac{\partial^2 U}{\partial Z^2} = \alpha \sum_k k[p_k I_1(kR) - p_k^* K_1(kR)]\mathrm{e}^{\mathrm{i}kZ} + \text{c.c.} \\ &\frac{1}{R}\frac{\partial}{\partial R}\left(R\frac{\partial V}{\partial R}\right) + \frac{\partial^2 V}{\partial Z^2} = \alpha \sum_k \mathrm{i}k[p_k I_0(kR) + p_k^* K_0(kR)]\mathrm{e}^{\mathrm{i}kZ} + \text{c.c.} \end{aligned}\right\} \tag{3.6}$$

with $\alpha = 1$ for the inner fluid and $\alpha = \lambda$ for the outer fluid. Solutions to this system of equations are computed as the superposition of the solution to the homogeneous equation and a particular solution having the same axial dependance, that is

$$\left.\begin{aligned} U(R, Z) &= U^{hom}(R, Z) + \alpha \sum_k f_k(R)\mathrm{e}^{\mathrm{i}kZ} + \text{c.c.} \\ V(R, Z) &= V^{hom}(R, Z) + \alpha \sum_k g_k(R)\mathrm{e}^{\mathrm{i}kZ} + \text{c.c.} \end{aligned}\right\}. \tag{3.7}$$

The solutions to the homogeneous equation are easily solved as

$$\left.\begin{aligned} U^{hom}(R,Z) &= \sum_k [u_k I_1(kR) + u_k^* K_1(kR)]\mathrm{e}^{\mathrm{i}kZ} + \text{c.c.} \\ V^{hom}(R,Z) &= \sum_k [v_k I_0(kR) + v_k^* K_0(kR)]\mathrm{e}^{\mathrm{i}kZ} + \text{c.c.} \end{aligned}\right\} \tag{3.8}$$

while the functions f_k, g_k are found to be

$$\left.\begin{aligned} f_k(R) &= \frac{p_k}{2} R I_0(kR) + \frac{p_k^*}{2} R K_0(kR) \\ g_k(R) &= \frac{\mathrm{i}p_k}{2} R I_1(kR) - \frac{\mathrm{i}p_k^*}{2} R K_1(kR) \end{aligned}\right\}. \tag{3.9}$$

Imposing that the inner hydrodynamical fields are finite at $R=0$ gives $u_k^* = v_k^* = p_k^*$ for the inner solution, while imposing that outer hydrodynamical fields are finite when $R \to \infty$ gives $u_k = v_k = p_k$ for the outer solution.

Thus, the inner solution reads

$$\left.\begin{aligned} U^{in}(R,Z) &= \sum_k \left[u_k I_1(kR) + \frac{p_k}{2} R I_0(kR) \right] \mathrm{e}^{\mathrm{i}kZ} + \text{c.c.} \\ V^{in}(R,Z) &= \sum_k \left[v_k I_0(kR) + \frac{\mathrm{i}p_k}{2} R I_1(kR) \right] \mathrm{e}^{\mathrm{i}kZ} + \text{c.c.} \\ P^{in}(R,Z) &= \sum_k p_k I_0(kR)\mathrm{e}^{\mathrm{i}kZ} + \text{c.c.} \end{aligned}\right\} \tag{3.10}$$

while the outer solution reads

$$\left.\begin{aligned} U^{out}(R,Z) &= \sum_k \left[u_k^* K_1(kR) + \lambda \frac{p_k^*}{2} R K_0(kR) \right] \mathrm{e}^{\mathrm{i}kZ} + \text{c.c.} \\ V^{out}(R,Z) &= \sum_k \left[v_k^* K_0(kR) - \lambda \frac{\mathrm{i}p_k^*}{2} R K_1(kR) \right] \mathrm{e}^{\mathrm{i}kZ} + \text{c.c.} \\ P^{out}(R,Z) &= \sum_k p_k^* K_0(kR)\mathrm{e}^{\mathrm{i}kZ} + \text{c.c.} \end{aligned}\right\}. \tag{3.11}$$

The incompressibility condition (2.15) imposes

$$\left.\begin{aligned} p_k + u_k k + \mathrm{i}v_k k &= 0 \\ \lambda p_k^* - u_k^* k + \mathrm{i}v_k^* k &= 0 \end{aligned}\right\}. \tag{3.12}$$

3.2. *Interfacial conditions*

We now turn to the coupling conditions, which can be formally written for any physical quantity g as

$$g(1 + \delta R(Z), Z) = 0 \quad \text{for all } Z.$$

Expanding g in powers of δR leads to

$$g^{\delta R}(1,Z) + \delta R \frac{\partial g^0}{\partial R}(1,Z) + O(\|\delta R\|^2) = 0 \quad \text{for all } Z.$$

Since there is no spatial variation in the base state, the coupling conditions simply write $g^{\delta R}(1, Z) = 0$ at leading order.

First, the coefficients of the external flow field are expressed as a function of the coefficients of the internal flow field by writing the continuity condition at the interface (2.2):

$$\begin{cases} U^{in}(1,Z) = U^{out}(1,Z) \\ V^{in}(1,Z) = V^{out}(1,Z) \end{cases} \Leftrightarrow \begin{cases} u_k I_1(k) + \dfrac{p_k}{2} I_0(k) = u_k^* K_1(k) + \lambda \dfrac{p_k^*}{2} K_0(k) \\ v_k I_0(k) + \dfrac{\mathrm{i} p_k}{2} I_1(k) = v_k^* K_0(k) - \lambda \dfrac{\mathrm{i} p_k^*}{2} K_1(k). \end{cases} \tag{3.13}$$

For a velocity field satisfying the incompressibility condition ($\boldsymbol{\nabla} \cdot \boldsymbol{v} = 0$), the surface incompressibility constraint ($\boldsymbol{\nabla}_s \cdot \boldsymbol{v} = 0$) can be rewritten as

$$\boldsymbol{n} \cdot \boldsymbol{D} \cdot \boldsymbol{n}_{|R=1} = 0$$

where $\boldsymbol{D} = 1/2(\boldsymbol{\nabla} \boldsymbol{v} + \boldsymbol{\nabla}^{\mathrm{T}} \boldsymbol{v})$ is the rate of deformation tensor. To leading order, the normal to the surface is given by $\boldsymbol{n} = \boldsymbol{e_r}$, thus surface incompressibility constraint can be written as

$$\frac{\partial U}{\partial R}_{|R=1} = 0 \Rightarrow \sum_k \left[u_k (I_0(k)k - I_1(k)) + \frac{p_k}{2} (I_0(k) + k I_1(k)) \right] \mathrm{e}^{\mathrm{i}kZ} + \text{c.c.} = 0.$$

Thus, the surface incompressibility constraint relates u_k to p_k, as well as u_k^* and p_k^*:

$$\left.\begin{aligned} u_k &= \frac{p_k}{2} \left[\frac{k I_1(k) + I_0(k)}{I_1(k) - k I_0(k)} \right] \\ u_k^* &= -\lambda \frac{p_k^*}{2} \left[\frac{k K_1(k) - K_0(k)}{K_1(k) + k K_0(k)} \right] \end{aligned}\right\}. \tag{3.14}$$

Using these relationships together with the continuity of the radial velocity allows one to express the outer pressure coefficients p_k^* as a function of p_k:

$$p_k^* = \frac{p_k}{\lambda} \frac{[2I_0(k)I_1(k) + k(I_1^2(k) - I_0^2(k))][K_1(k) + kK_0(k)]}{[2K_0(k)K_1(k) - k(K_1^2(k) - K_0^2(k))][I_1(k) - kI_0(k)]}. \tag{3.15}$$

To leading order, the mechanical equilibrium in the tangential direction reads

$$\frac{\mathrm{d}\Gamma}{\mathrm{d}Z} - \left[\frac{\partial V^{in}}{\partial R} - \frac{1}{\lambda} \frac{\partial V^{out}}{\partial R} + \left(\frac{\partial U^{in}}{\partial Z} - \frac{1}{\lambda} \frac{\partial U^{out}}{\partial Z} \right) \right]_{R=1} = 0. \tag{3.16}$$

Integration of the previous equation with respect to Z allows us to determine the tension:

$$\Gamma(Z) = \Gamma_0 + \sum_{k \neq 0} \mathrm{e}^{\mathrm{i}kZ} \left[\left(u_k I_1(k) - \frac{u_k^*}{\lambda} K_1(k) - \mathrm{i} v_k I_1(k) - \mathrm{i} \frac{v_k^*}{\lambda} K_1(k) \right) + p_k I_0(k) - p_k^* K_0(k) \right]. \tag{3.17}$$

Using the incompressibility equation to eliminate v_k, v_k^* and then the continuity of the radial velocity leads to

$$\Gamma(Z) = \Gamma_0 + \sum_{k \neq 0} \mathrm{e}^{\mathrm{i}kZ} \left[\frac{p_k I_1(k) + p_k^* K_1(k)}{k} + \left(1 - \frac{1}{\lambda} \right) (2u_k I_1(k) + p_k I_0(k)) \right]. \tag{3.18}$$

To leading order, the mechanical equilibrium in the normal direction reads

$$P^{in} - P^{out} + \left[\frac{2}{\lambda}\frac{\partial U^{out}}{\partial R} - 2\frac{\partial U^{in}}{\partial R}\right]_{R=1} + 2\Gamma H - \frac{1}{\Gamma^0}[2\Delta_s H + 4H(H^2 - K)] = 0. \quad (3.19)$$

Using the surface incompressibility constraint ($\partial U/\partial R|_{R=1} = 0$) provides one of the key equations:

$$\sum_k (p_k I_0(k) - p_k^* K_0(k))\mathrm{e}^{\mathrm{i}kZ} = \sum_k \left[\delta R_k \left(\frac{k^4}{\Gamma^0} - k^2\left(\frac{1}{2\Gamma^0} - 1\right) + \left(\frac{3}{2\Gamma^0} - 1\right)\right) + \Gamma_k\right]\mathrm{e}^{\mathrm{i}kZ} \quad (3.20)$$

where the right-hand side corresponds to the first-order expansion of membrane forces (see appendix A). Injecting the expression of Γ_k determined by (3.18) leads to

$$\begin{aligned} p_k \;=\; & \left(k\left[\delta R_k\left(\frac{k^4}{\Gamma^0} - k^2\left(\frac{1}{2\Gamma^0} - 1\right) + \left(\frac{3}{2\Gamma^0} - 1\right)\right)\right](kI_0 - I_1)\left[2K_1K_0 - k(K_1^2 - K_0^2)\right]\right) \\ & \times \left((1+k^2)\left[I_1^2(2K_0K_1 - k(K_1^2 - K_0^2)) + \frac{1}{\lambda}K_1^2(2I_0I_1 + k(I_1^2 - I_0^2))\right]\right)^{-1} \end{aligned} \quad (3.21)$$

where, for clarity, we have omitted the argument of the Bessel functions and thus note $I_0 = I_0(k), I_1 = I_1(k), \ldots$. This notation will be kept in the following.

Finally, the growth rate is determined by the evaluation of the radial velocity:

$$\frac{\partial \delta R_k}{\partial t} = u_k I_1 + \frac{p_k}{2} I_0 \quad (3.22)$$

which leads to

$$\begin{aligned} \sigma_k \;=\; & -\left(k\left(\frac{k^4}{\Gamma^0} - k^2\left(\frac{1}{2\Gamma^0} - 1\right) + \left(\frac{3}{2\Gamma^0} - 1\right)\right)\right) \\ & \times \left(2(1+k^2)\left[\frac{I_1^2}{\left[2I_1I_0 - k(I_0^2 - I_1^2)\right]} + \frac{K_1^2}{\lambda\left[2K_1K_0 - k(K_1^2 - K_0^2)\right]}\right]\right)^{-1} \end{aligned} \quad (3.23)$$

which is the main result of this paper. To ease the comparison with previous results (Nelson *et al.* 1995; Goldstein *et al.* 1996; Gurin *et al.* 1996; Powers 2010), we also write the growth rate (3.23) for $\lambda = 1$ (no viscosity contrast) using $(I_0K_1 + I_1K_0) = 1/k$ (wronskian of $\{I_0, K_0\}$, see e.g. Abramowitz & Stegun 1972) which leads to

$$\begin{aligned} \overline{\sigma_k} \;=\; & -\left(\left(\frac{k^4}{\Gamma^0} - k^2\left(\frac{1}{2\Gamma^0} - 1\right) + \left(\frac{3}{2\Gamma^0} - 1\right)\right)(k(I_0^2 - I_1^2) - 2I_0I_1)(k(K_0^2 - K_1^2) + 2K_0K_1)\right) \\ & \times \left(2[2K_1I_1 + k(I_1K_0 - I_0K_1)]\frac{(1+k^2)}{k^2}\right)^{-1}. \end{aligned} \quad (3.24)$$

4. Discussion

4.1. *Comparison with previous works*

The expression found previously for the growth rate differs markedly from the results reported by Nelson *et al.* (1995), Goldstein *et al.* (1996), Gurin *et al.* (1996) and Powers (2010). However, if we do not include variations of tension and set $\Gamma_k = 0$,

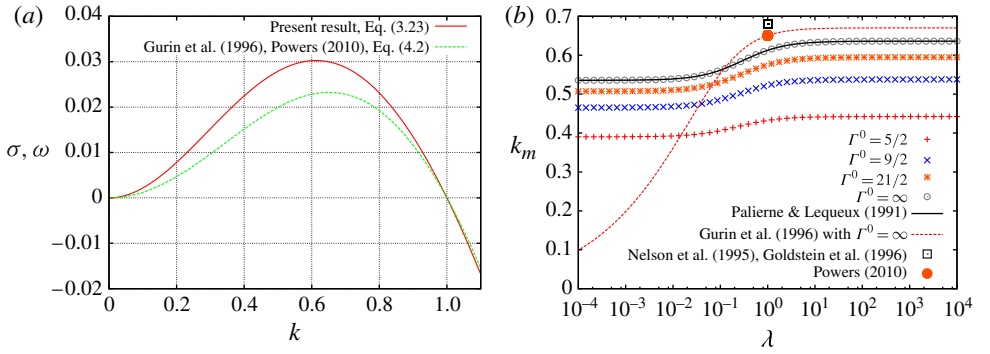

FIGURE 3. (Colour online) (*a*) Comparison of the growth rate derived in the present paper (3.24) with previous results neglecting gradients of tension (Gurin *et al.* 1996; Powers 2010), see (4.2), in the limit of infinite tension. (*b*) Evolution of the most unstable wavenumber k_{max} with the viscosity contrast λ for several values of the dimensionless tension Γ^0.

we find a growth rate given by

$$\omega_k = \left(\frac{k^4}{\Gamma^0} - k^2\left(\frac{1}{2\Gamma^0} - 1\right) + \left(\frac{3}{2\Gamma^0} - 1\right)\right) \times \left(2\left[\frac{I_0(I_1 - kI_0)}{\left[2I_1I_0 - k(I_0^2 - I_1^2)\right]} - \frac{K_0(K_1 + kK_0)}{\lambda\left[2K_1K_0 - k(K_1^2 - K_0^2)\right]}\right]\right)^{-1} \tag{4.1}$$

which is exactly (3.8) of Gurin *et al.* (1996). To compare with Powers (2010), we set $\lambda = 1$ in (4.1) and use once more $(I_0K_1 + I_1K_0) = 1/k$ to find

$$\overline{\omega_k} = -\left(\left(\frac{k^4}{\Gamma^0} - k^2\left(\frac{1}{2\Gamma^0} - 1\right) + \left(\frac{3}{2\Gamma^0} - 1\right)\right)(k(I_0^2 - I_1^2) - 2I_0I_1)(k(K_0^2 - K_1^2) + 2K_0K_1)\right) \times (2[I_1K_1 + I_0K_0 + k(I_0K_1 - I_1K_0)])^{-1} \tag{4.2}$$

which is the result reported by Powers (2010) if the membrane viscosity contribution is neglected. Comparison of (4.1) with (3.23) and (4.2) with (3.24) allows us to conclude that the contribution of tension gradients determined by mechanical equilibrium of the membrane in the tangent direction leads to a strong modification of the denominator of the growth rate. Note that the change is not simply a different combination of Bessel functions but comes also from a multiplicative term $k^2/(1+k^2)$. To highlight the quantitative difference, the dispersion relations (3.24) derived in this paper and (4.2) proposed by Gurin *et al.* (1996) and Powers (2010) are drawn in figure 3(*a*) in the case without viscosity contrast, $\lambda = 1$. The most unstable mode has roughly a 25 % higher growth rate for infinite tension. Note that this result is consistent with the analysis of the effect of variations of tension proposed in § 2.3: the difference between the growth rate computed here and previous results is entirely due to the inclusion of the gradients of tension, whose effect is to strengthen the instability. Physically, those gradients are necessary to ensure that both mechanical equilibrium in the tangent direction and surface incompressibility constraint are fulfilled.

Inclusion of the viscosity contrast, which was considered by Gurin *et al.* (1996), but not by Nelson *et al.* (1995), Goldstein *et al.* (1996) and Powers (2010), reveals a quantitative difference with our results as already mentioned but also a qualitative one. Indeed, our results show that the most unstable wavenumber k_{max} saturates in the limits of low and high viscosity contrast λ while it decreases strongly (see figure 3*b*) as λ tends to zero in Gurin *et al.* (1996). See § 4.3 for a discussion of the wavenumber.

4.2. *Incompressible interface limit*

Before discussing the properties of the pearling instability, it is worth noting that taking the limit of infinite tension of (3.23):

$$\lim_{\Gamma^0\to\infty} \sigma(k,\,\Gamma^0,\,\lambda) = (k[1-k^2]) \left(2(1+k^2) \left[\frac{I_1^2}{[2I_1I_0 - k(I_0^2 - I_1^2)]} + \frac{K_1^2}{\lambda\left[2K_1K_0 - k(K_1^2 - K_0^2)\right]} \right] \right)^{-1} \tag{4.3}$$

one recovers the result of Palierne and Lequeux in the limit of Newtonian fluids and incompressible interface (Palierne & Lequeux 1991, equation (70)) and the result of Timmermans and Lister in the limit of very viscous thread and strong surfactants effects (Timmermans & Lister 2002, equation (3.13)), with, using their notation, $\Re \to 0$, $\beta \to \infty$), which is a special case for $\lambda \to \infty$. The parameter β used by Timmermans & Lister (2002) is defined as the ratio between Gibbs elasticity and the homogeneous value of the surface tension. In the limit $\beta \to \infty$, as discussed in Timmermans & Lister (2002), surfactants tend to oppose any change of their surface densities: any such variation would lead to strong gradients of tension, which would in turn drive strong flows tending to restore homogenous state. Thus, the equation of conservation of surfactants reduces to (Hansen *et al.* 1999; Timmermans & Lister 2002)

$$\left[\frac{\partial V}{\partial Z} + \frac{U}{R} \right]_{|R=1} = 0 + O(\beta^{-1}) \tag{4.4}$$

which is exactly the surface divergence free constraint (2.5). It is interesting to note that this constraint is sufficient to prevent the growth of infinite wavelength perturbations, even in the case of a viscous thread in an inviscid environment (for which the Rayleigh analysis Rayleigh (1892*b*) gives $k_{max} = 0$).

The agreement between the analysis of the infinite tension behaviour (4.3) of the instability (3.23) and the incompressible interface limit provides an important element of validation of the calculation presented here. This limit is also physically important because relevant quantities as the most unstable wavenumber quickly saturate as a function of Γ^0: for $(\Gamma^0/(3/2) - 1) > 10$, variations of k_{max} are less than 5 %. In particular, as shown in figure 3(*b*), the value of the most unstable wavenumber was overestimated by previous analyses (Nelson *et al.* 1995; Goldstein *et al.* 1996; Gurin *et al.* 1996; Powers 2010). However, experimentally (Bar-Ziv & Moses 1994; Bar-Ziv *et al.* 1997, 1998), the dimensionless distance to threshold $(2\Gamma^0/3 - 1)$ varies between 0 and 15, which gives a range of variation for Γ^0 between 3/2 and 24. In this range, both the most unstable wavenumber and the growth rate varies notably, which justifies to keep the bending rigidity in the analysis of the pearling instability.

4.3. *Pearling instability*

We now turn to the analysis of the pearling instability, with particular attention paid to the corrections our analysis brings to the previously reported results (Nelson *et al.* 1995; Goldstein *et al.* 1996; Gurin *et al.* 1996; Powers 2010).

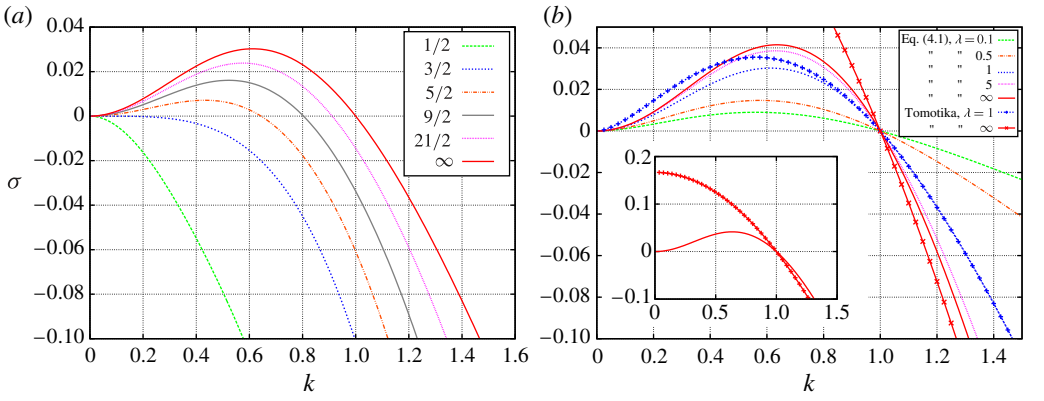

FIGURE 4. (Colour online) Dimensionless growth rate as a function of the dimensionless wave number for: (*a*) different values of the dimensionless tension Γ^0 and a unit viscosity contrast ($\lambda = 1$) and (*b*) different values of the viscosity contrast in the limit of an infinite tension ($\Gamma^0 \to \infty$). The classical Rayleigh–Plateau instability is also plotted for $\lambda = 1$ and $\lambda \to \infty$ using the result of Tomotika (1935). (Inset) For $\lambda \to \infty$, the Rayleigh–Plateau instability is maximal for $k = 0$, with $\sigma(0) = 1/6 \approx 0.1667$, well above the maximal value of σ_k for a cylindrical vesicle.

The denominator of (3.23) is always positive, thus the sign of the growth rate is entirely determined by the numerator: for $\Gamma^0 < 3/2$, all wave numbers are damped, while for $\Gamma^0 > 3/2$, there is a band of unstable wavenumbers between $[0, k_0]$, with k_0 given by

$$k_0 = \left(\frac{1}{4} - \frac{\Gamma^0}{2} + \frac{1}{4}\sqrt{4(\Gamma^0)^2 + 12\Gamma^0 - 23} \right)^{1/2} \tag{4.5}$$

which tends towards 1 as $\Gamma^0 \to \infty$. While the threshold $\Gamma^0 = 3/2$ (or $\gamma^0 = 3\kappa/2r_0^2$) has already been determined by Goldstein *et al.* (1996) and Gurin *et al.* (1996), the marginal mode k_0 was not derived. This dimensionless wavenumber depends only on the membrane dimensionless tension, since it represents the separation between stable and unstable wavenumbers: for small tension, bending rigidity tends to stabilize wavenumbers higher than k_0, while for high tension, one recovers the result of Plateau (1873), that is, unstable wavelengths are those higher than the perimeter of the cylinder. As a consequence, it does not depend on the viscosity contrast.

In this band of unstable wavenumbers, the growth rate is positive and exhibits a maximum for k_{max} (see figure 4). The position of the maximum depends both on viscosity contrast and tension, as shown in figure 5: it increases in a monotonic way with both the tension and the viscosity contrast. This maximum saturates around a value of $k_{max} \approx 0.613$ for $\lambda = 1$ and $k_{max} \approx 0.636$ for $\lambda \to \infty$. This shows the notable influence of the membrane on the dynamics of the instability, even in the large tension regime: for the classical Rayleigh–Plateau instability in the viscous case, Tomotika (1935) gives $k_{max} = 0.563$ for $\lambda = 1$ and $k_{max} = 0$ for $\lambda \to \infty$. As shown in figure 3(*b*), these values are lower than the $k_{max} \approx 0.68$ for $\lambda = 1$ reported by Nelson *et al.* (1995) and Goldstein *et al.* (1996), and than the value $k_{max} \approx 0.651$ computed from the growth rate given in Gurin *et al.* (1996) and Powers (2010).

While the limits of low and high viscosity contrast are more formal than physically relevant, it is interesting to note that there is a noticeable variation (see figure 3*b*) of

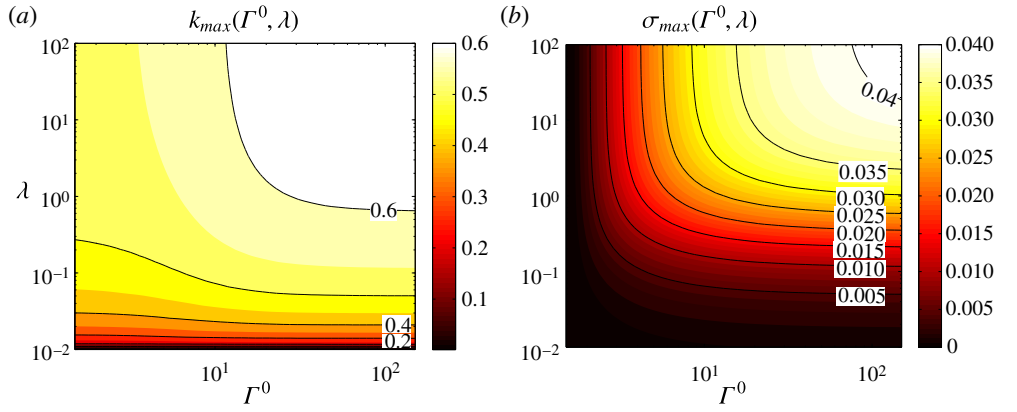

FIGURE 5. (Colour online) (*a*) Evolution of the most unstable wavenumber k_{max} with the dimensionless tension Γ^0 and the viscosity contrast λ. (*b*) Evolution of the maximal growth rate as a function of viscosity contrast and dimensionless tension.

the most unstable wavenumber for viscosity contrast in the experimentally accessible range of $\lambda \in [0.01, 10]$: for $\lambda = 0.1$, $k_{max} = 0.56$, for $\lambda = 1$, $k_{max} = 0.61$, while for $\lambda = 10$, $k_{max} = 0.63$. This leads to roughly 10 % variation of the dimensionless wavenumber associated with the most unstable mode.

5. Conclusion

The linear stability analysis of a viscous cylindrical thread immersed into a viscous fluid with a phospholipidic membrane under tension γ^0 has been performed, assuming small deviations from the cylindrical reference shape. The thread is found to be stable for all wavenumbers when the tension is below a critical value of $3\kappa/(2r_0^2)$, with κ the bending modulus of the membrane, and r_0 the radius of the unperturbed cylinder. If the tension exceeds this critical value, the thread is unstable with respect to perturbations of its radius with a wavenumber in the band $[0, k_0]$, where k_0 is given by (4.5), and depends on the tension γ^0, but not on the viscosity contrast λ. In the limit of infinite tension, $k_0 \to 1$. The growth rate of perturbations is given by (3.23), which shows that even in the limit of infinite tension, the presence of the membrane at the interface leads to strong deviation from the standard Rayleigh–Plateau case with viscous fluids (Tomotika 1935). In particular, in this limit, the system behaves as an interface covered with strong surfactants, preventing the growth of small wavenumbers disturbances (Palierne & Lequeux 1991; Timmermans & Lister 2002). This is because strong surfactants effects oppose any variation of the surfactant density, leading to an effectively surface incompressible interface. The wavenumber with the maximal growth rate depends both on the applied tension and on the viscosity contrast. For a cylindrical vesicle with matched viscosity fluids ($\lambda = 1$), the most unstable wavelength is $l_{max} = (2\pi/k_{max})r_0$ with r_0 the radius of the unperturbed cylinder. A perturbation of wavelength l_{max} is amplified with a growth rate $\sigma = \sigma_{max}\gamma^0/(\eta r_0)$ with γ^0 the imposed tension and η the viscosity of the fluids. Using typical experimental value of $r_0 \approx 0.5$ μm, $\gamma^0 \approx 5 \times 10^{-6}$ J m^{-2} leads to $l_{max} \approx 5.4$ μm, in qualitative agreement with experimental results (Bar-Ziv & Moses 1994; Bar-Ziv *et al.* 1997, 1998) and a growth rate of $\sigma_{max} \approx 2 \times 10^1$ s^{-1}. Quantitative comparisons with experimental results are more difficult since thermal fluctuations of the membrane prevent measurements

of the linear stage of the instability (Bar-Ziv *et al.* 1997). The values of the dimensionless selected wavenumber in experiments (Bar-Ziv & Moses 1994; Bar-Ziv *et al.* 1997, 1998) varies from $k = 0.47$ close to threshold ($\Gamma^0 \approx 2$) to roughly $k = 1$ for a dimensionless tension $\Gamma^0 \approx 23$. In this range of tension, the dimensionless most unstable wavenumber computed with (3.23) varies from 0.37 to 0.60, while the dimensionless marginal wavenumber computed with (4.5) varies from 0.54 to 0.96. To quantitatively compare with experiments, an extension of the present linear theory to the next order would be necessary to describe nonlinear effects. Inclusion in the theory of the membrane viscosity could also be necessary to describe more accurately the vesicle membrane.

Acknowledgements

This work has benefited of financial support from the ANR CAPSHYDR (11-BS09-013-02), from the ANR Polytransflow (13-BS09-0015-01), from Labex MEC (ANR-11-LABX-0092), from A*MIDEX (ANR-11-IDEX-0001-02) and from CNES.

Appendix. Differential geometry in cylindrical coordinates

In this section, we derive geometrical quantities (metric, curvature, forces, ...) useful for the linear stability analysis (§ 3). We consider the shape of the tube to be described in cylindrical coordinates by

$$\boldsymbol{x}(\theta, z) = R(Z)\boldsymbol{e_r} + Z\boldsymbol{e_z} = R(Z)[\cos\theta \boldsymbol{e_x} + \sin\theta \boldsymbol{e_y}] + Z\boldsymbol{e_z}. \tag{A 1}$$

Tangent to the shape are given by derivatives with respect to parametrization:

$$\left.\begin{aligned} \boldsymbol{t_Z} &= \frac{\partial \boldsymbol{x}}{\partial Z} = R'(Z)\boldsymbol{e_r} + \boldsymbol{e_z} \\ \boldsymbol{t_\theta} &= \frac{\partial \boldsymbol{x}}{\partial \theta} = R(Z)\left[-\sin\theta \boldsymbol{e_x} + \cos\theta \boldsymbol{e_y}\right] \end{aligned}\right\}. \tag{A 2}$$

Thus, metric coefficients follows easily:

$$\left.\begin{aligned} g_{ZZ} &= \boldsymbol{t_Z}\cdot\boldsymbol{t_Z} = 1 + R'(Z)^2 \\ g_{\theta\theta} &= \boldsymbol{t_\theta}\cdot\boldsymbol{t_\theta} = R(Z)^2 \\ g_{\theta Z} &= g_{Z\theta} = 0 \end{aligned}\right\} \tag{A 3}$$

as well as the outward normal

$$\boldsymbol{n} = \frac{\boldsymbol{t_\theta}\wedge\boldsymbol{t_Z}}{\sqrt{g}} = \frac{1}{\left(1+R'^2\right)^{1/2}}[\boldsymbol{e_r} - R'\boldsymbol{e_z}]. \tag{A 4}$$

Curvature tensor coefficients are computed as $b_{\alpha\beta} = \boldsymbol{n}\cdot\partial\boldsymbol{t_\alpha}/\partial\beta$, leading to

$$\left.\begin{aligned} 2H &= \frac{R''}{(1+R'^2)^{3/2}} - \frac{1}{R(1+R'^2)^{1/2}} \\ K &= \frac{-R''}{R(1+R'^2)^2} \end{aligned}\right\}, \tag{A 5}$$

where H is the mean curvature and K is the Gaussian curvature. Finally, it is useful to define surface operators as follows:

$$\left.\begin{aligned} \boldsymbol{\nabla}_s f &= \frac{\partial f}{\partial Z}\boldsymbol{t}^{\boldsymbol{Z}} \\ \boldsymbol{\nabla}_s \cdot \boldsymbol{v} &= \frac{U}{R} + \left(\frac{\partial U}{\partial Z}\frac{\partial R}{\partial Z} + \frac{\partial V}{\partial Z}\right) g^{zz} \\ \Delta_s f &= \frac{1}{\sqrt{g}}\frac{\partial}{\partial z}\left(\sqrt{g} g^{zz}\frac{\partial f}{\partial z}\right) \end{aligned}\right\}. \tag{A 6}$$

We then specialize these relations to the case of $R(Z) = 1 + \delta R(Z)$ where $\delta R(Z)$ is the dimensionless deviation of the shape from the cylinder. For a linear stability analysis, it is sufficient to compute geometrical quantities up to $O(\|\delta R\|^2)$. We have

$$\left.\begin{aligned} &\boldsymbol{t_Z} = \delta R' \boldsymbol{e_r} + \boldsymbol{e}_z, \quad \boldsymbol{t}^{\boldsymbol{Z}} = \delta R' \boldsymbol{e_r} + \boldsymbol{e}_z + O(\|\delta R\|^2), \quad \boldsymbol{n} = \boldsymbol{e_r} - \delta R' \boldsymbol{e}_z + O(\|\delta R\|^2) \\ &H = \delta R'' - (1 - \delta R) + O(\|\delta R\|^2), \quad K = -\delta R'' + O(\|\delta R\|^2) \\ &\Delta_s H = \delta R'''' + \delta R'' + O(\|\delta R\|^2), \quad \boldsymbol{\nabla}_s \Gamma = \Gamma' \boldsymbol{e_z} \end{aligned}\right\}. \tag{A 7}$$

REFERENCES

ABRAMOWITZ, M. & STEGUN, I. A. (ed.) 1972 In *Handbook of Mathematical Functions with Formulas, Graphs, and Mathematical Tables* Dover Publications.

AMAROUCHENE, Y., BONN, D., MEUNIER, J. & KELLAY, H. 2001 Inhibition of the finite-time singularity during droplet fission of a polymeric fluid. *Phys. Rev. Lett.* **86**, 3558–3561.

ARDEKANI, A. M., SHARMA, V. & MCKINLEY, G. H. 2010 Dynamics of bead formation, filament thinning and breakup in weakly viscoelastic jets. *J. Fluid Mech.* **665**, 46–56.

BAR-ZIV, R. & MOSES, E. 1994 Instability and 'pearling' states produced in tubular membranes by competition of curvature and tension. *Phys. Rev. Lett.* **73**, 1392–1395.

BAR-ZIV, R., MOSES, E. & NELSON, P. 1998 Dynamic excitations in membranes induced by optical tweezers. *Biophys. J.* **75** (1), 294–320.

BAR-ZIV, R., TLUSTY, T. & MOSES, E. 1997 Critical dynamics in the pearling instability of membranes. *Phys. Rev. Lett.* **79**, 1158–1161.

BAR-ZIV, R., TLUSTY, T., MOSES, E., SAFRAN, S. A. & BERSHADSKY, A. 1999 Pearling in cells: a clue to understanding cell shape. *Proc. Natl Acad. Sci.* **96** (18), 10140–10145.

BHAT, P. P., APPATHURAI, S., HARRIS, M. T., PASQUALI, M., MCKINLEY, G. H. & BASARAN, O. A. 2010 Formation of beads-on-a-string structures during break-up of viscoelastic filaments. *Nat. Phys.* **6**, 625–631.

BOEDEC, G., JAEGER, M. & LEONETTI, M. 2013 Sedimentation-induced tether on a settling vesicle. *Phys. Rev.* E **88**, 010702.

CAMPELO, F. & HERNÁNDEZ-MACHADO, A. 2007 Model for curvature-driven pearling instability in membranes. *Phys. Rev. Lett.* **99**, 088101.

CHAÏEB, S. & RICA, S. 1998 Spontaneous curvature-induced pearling instability. *Phys. Rev.* E **58**, 7733–7737.

CLASEN, C., EGGERS, J., FONTELOS, M. A., LI, J. & MCKINLEY, G. H. 2006 The beads-on-string structure of viscoelastic threads. *J. Fluid Mech.* **556**, 283–308.

DIMOVA, R., ARANDA, S., BEZLYEPKINA, N., NIKOLOV, V., RISKE, K. A. & LIPOWSKY, R. 2006 A practical guide to giant vesicles. probing the membrane nanoregime via optical microscopy. *J. Phys.: Condens. Matter* **18** (28), S1151.

EGGERS, J. & VILLERMAUX, E. 2008 Physics of liquid jets. *Rep. Prog. Phys.* **71** (3), 036601.

EVANS, E., BOWMAN, H., LEUNG, A., NEEDHAM, D. & TIRRELL, D. 1996 Biomembrane templates for nanoscale conduits and networks. *Science* **273** (5277), 933–935.

FYGENSON, D. K., MARKO, J. F. & LIBCHABER, A. 1997 Mechanics of microtubule-based membrane extension. *Phys. Rev. Lett.* **79**, 4497–4500.

GOLDSTEIN, R. E., NELSON, P., POWERS, T. & SEIFERT, U. 1996 Front propagation in the pearling instability of tubular vesicles. *J. Phys. II France* **6**, 767–796.

GOVEAS, J. L., MILNER, S. T. & RUSSEL, W. B. 1997 Late stages of the 'pearling' instability in lipid bilayers. *J. Phys. II France* **7** (9), 1185–1204.

GRANEK, R. & OLAMI, Z. 1995 Dynamics of Rayleigh-like instability induced by laser tweezers in tubular vesicles of self-assembled membranes. *J. Phys. II France* **5** (9), 1349–1370.

GURIN, K. L., LEBEDEV, V. V. & MURATOV, A. A. 1996 Dynamic instability of a membrane tube. *J. Expl Theor. Phys.* **83** (2), 321–326.

HANSEN, S., PETERS, G. W. M. & MEIJER, H. E. H. 1999 The effect of surfactant on the stability of a fluid filament embedded in a viscous fluid. *J. Fluid Mech.* **382**, 331–349.

KANTSLER, V., SEGRE, E. & STEINBERG, V. 2008 Critical dynamics of vesicle stretching transition in elongational flow. *Phys. Rev. Lett.* **101**, 048101.

MÉNAGER, C., MEYER, M., CABUIL, V., CEBERS, A., BACRI, J. -C. & PERZYNSKI, R. 2002 Magnetic phospholipid tubes connected to magnetoliposomes: pearling instability induced by a magnetic field. *Eur. Phys. J.* E **7** (4), 325–337.

NELSON, P., POWERS, T. & SEIFERT, U. 1995 Dynamical theory of the pearling instability in cylindrical vesicles. *Phys. Rev. Lett.* **74**, 3384–3387.

OLIVEIRA, M. S. N. & MCKINLEY, G. H. 2005 Iterated stretching and multiple beads-on-a-string phenomena in dilute solutions of highly extensible flexible polymers. *Phys. Fluids* **17** (7), 071704.

OLMSTED, P. D. & MACINTOSH, F. C. 1997 Instability and front propagation in laser-tweezed lipid bilayer tubules. *J. Phys. II France* **7** (1), 139–156.

PALIERNE, J. F & LEQUEUX, F. 1991 Sausage instability of a thread in a matrix; linear theory for viscoelastic fluids and interface. *J. Non-Newtonian Fluid Mech.* **40** (3), 289–306.

PLATEAU, J. 1873 *Statique Expérimentale et Théorique des Liquides Soumis aux Seules Forces Moléculaires*. Gauthier-Villars.

POWERS, T. R. 2010 Dynamics of filaments and membranes in a viscous fluid. *Rev. Mod. Phys.* **82**, 1607–1631.

POWERS, T. R. & GOLDSTEIN, R. E. 1997 Pearling and pinching: propagation of Rayleigh instabilities. *Phys. Rev. Lett.* **78**, 2555–2558.

RAYLEIGH, L. 1878 On the instability of jets. *Proc. Lond. Math. Soc.* **s1–10** (1), 4–13.

RAYLEIGH, L. 1892*a* XIX. On the instability of cylindrical fluid surfaces. *Phil. Mag. Ser. 5* **34** (207), 177–180.

RAYLEIGH, L. 1892*b* XVI. On the instability of a cylinder of viscous liquid under capillary force. *Phil. Mag. Ser. 5* **34** (207), 145–154.

SANBORN, J., OGLECKA, K., KRAUT, R. S. & PARIKH, A. N. 2013 Transient pearling and vesiculation of membrane tubes under osmotic gradients. *Faraday Discuss.* **161**, 167–176.

TIMMERMANS, M.-L. E. & LISTER, J. R. 2002 The effect of surfactant on the stability of a liquid thread. *J. Fluid Mech.* **459**, 289–306.

TOMOTIKA, S. 1935 On the instability of a cylindrical thread of a viscous liquid surrounded by another viscous fluid. *Proc. R. Soc. Lond.* A **150** (870), 322–337.

TSAFRIR, I., SAGI, D., ARZI, T., GUEDEAU-BOUDEVILLE, M.-A., FRETTE, V., KANDEL, D. & STAVANS, J. 2001 Pearling instabilities of membrane tubes with anchored polymers. *Phys. Rev. Lett.* **86**, 1138–1141.

VLAHOVSKA, P., PODGORSKI, T. & MISBAH, C. 2009 Vesicles and red blood cells in flow: from individual dynamics to rheology. *C. R. Phys.* **10** (8), 775–789.

WHITAKER, S. 1976 Studies of the drop-weight method for surfactant solutions: III. Drop stability, the effect of surfactants on the stability of a column of liquid. *J. Colloid Interface Sci.* **54** (2), 231–248.

YANAGISAWA, M., IMAI, M. & TANIGUCHI, T. 2008 Shape deformation of ternary vesicles coupled with phase separation. *Phys. Rev. Lett.* **100**, 148102.

ZHAO, H. & SHAQFEH, E. S. G. 2013 The shape stability of a lipid vesicle in a uniaxial extensional flow. *J. Fluid Mechan.* **719**, 345–361.